Received 14 December 2024; revised 22 January 2025; accepted 20 February 2025. Date of publication 27 February 2025; date of current version 17 March 2025.

Digital Object Identifier 10.1109/OJCOMS.2025.3546566

60-GHz Propagation Measurement and Modeling: Indoor and Outdoor With Extreme Winter Environments

SATZHAN S. ASKAROV[1], REFIK C. KIZILIRMAK[1] (Senior Member, IEEE), BEHROUZ MAHAM[1] (Senior Member, IEEE), AND IKECHI AUGUSTINE UKAEGBU[1,2] (Senior Member, IEEE)

[1]Department of Electrical and Computer Engineering, Nazarbayev University, 010000 Astana, Kazakhstan
[2]Division of Engineering Technology, University of West Alabama, Livingston, AL 35470, USA

CORRESPONDING AUTHOR: I. A. UKAEGBU (e-mail: iukaegbu@uwa.edu)

This work was supported by the Faculty Development Competitive Research Grant Program of Nazarbayev University under Grant 20122022FD4125.

ABSTRACT A thorough understanding of how 60 GHz millimeter-wave communication systems behave in severe weather conditions is essential due to the growing use of these technologies in outdoor settings. However, there has been limited research on how snowstorms affect millimeter-wave power propagation, which makes designing and relying on such systems difficult. Motivated by the need to create robust communication solutions for harsh climates, this work investigates the behavior of 60 GHz millimeter-wave power transmission under outdoor snowstorm settings, therefore addressing this gap. The research examines the impact of different transmitter-receiver (T-R) distances on received power under snowstorm conditions, characterized by an 18 m/s wind speed, 86% humidity, 0.2 mm/h snowfall rate, 1009.8 mbar atmospheric pressure, and $-7°C$ temperature, and compares the received power with that in indoor room conditions. Our findings reveal a significant reduction in received power in snowstorm environments compared to indoor settings. Specifically, at T-R distances of approximately 1 meter, the received power in a snowstorm was observed to be approximately 15 dBm lower than indoors. Furthermore, as the T-R distance is extended to 7 meters, this contrast is nearly halved, with the outdoor received power registering approximately 7 dBm less than the indoor conditions. These results underscore the considerable influence of snowstorm conditions on 60 GHz millimeter-wave power propagation and emphasize the necessity of comprehending these effects for outdoor communication systems operating in such environments. The study also provides insights into how the path-loss equation can be modified for snowstorm scenarios.

INDEX TERMS Path-loss estimate, mmWave communications, 5G, communications under snowstorm.

I. INTRODUCTION

NOWADAYS, the explosion of mobile data and the widespread use of smartphones present new issues for wireless service providers in managing bandwidth shortages on a worldwide scale. Herein, the huge available bandwidth at millimeter wave (mmWave) frequencies makes them appealing for 5th-generation cellular networks [1]. Many commercial wireless systems like IEEE 802.11ad, a 60 GHz band Multiple Gigabit Wireless System (MGWS) standard for local area networking, have previously investigated the unlicensed mmWave bands [2]. mmWave communication can revolutionize commercial wireless systems by increasing data rates and capacity and opening new frontiers in energy harvesting, physical layer security, and Terahertz (THz) research for 5G applications and beyond [3]. Moreover, with their continued development, mmWave technologies will be able to meet the new demands of 6G systems while still facilitating the ultra-high-speed data transfer and low-latency services that 5G networks are known for [4]. MmWave communications can achieve several Gbps speeds in mobile networks, as noted in [5]. To unleash mmWave technology's full potential, the study also stresses the need to solve several technological issues before large-scale adoption. In addition to its use in mobile networks, mmWave technology can be

applied in advanced imaging systems, high-speed backhaul and vehicular communications, as highlighted in [6]. The synthesis of recent advances includes channel modeling, MIMO design, multiple access methods, performance analysis, standardization, and deployment strategies [5]. The authors of [7] analyze mmWave coverage and data rate using stochastic geometry to account for outdoor users and infrastructure. The study findings enclose that signal-to-noise-and-interference ratio (SINR) coverage is comparable to conventional Ultra-High Frequency (UHF) networks at high base station (BS) concentrations. They also infer that as BS density rises, power-limited regimes become interference-limited. The study by MacCartney and Rappaport [8] uncovered that 28 and 73 GHz bands could provide street-level coverage up to 200 meters employing low-power BS, even in urban canyons where Line-of-Sight (LOS) conditions are not present. Apart from the deployment issues, weather conditions also greatly influence the mmWave channels. Authors in [9] state that in the 60 GHz band, rain, fog, and snow significantly reduce mmWave signal power and coverage up to 60 meters. Thus, using mmWave bands presents considerable Path Loss (PL) and resulting BS deployment issues that must be addressed to ensure the reliability and effectiveness of future 5G wireless networks. Therefore, mmWave systems may achieve their full potential with careful examination and design.

Nevertheless, despite its potential to reach multi-gigabit speeds, mmWave communication undergoes major challenges due to being prone to environmental factors. Harsh weather phenomena like snowstorms can result in significant signal degradation, adversely affecting reliability and coverage. Hence, a particular interest is drawn to the investigation of the adverse weather effects on mmWave communication. To analyze the influence of severe weather in realistic circumstances, [9] tested mmWave communication on the road for traffic in a typical city setting (Paderborn city). Their results suggest that the maximum communication distance for 100 dB Path-loss is 71 m in clear weather, but it shrinks by 20 m in rain and snow. The impact of snowfall in the Himalayan highlands on signal attenuation at 433 MHz was investigated in recent research by Garg and Soni [10]. However, in the lower band, their inferences still provide crucial insights into the influence of snow accumulation on the PL behavior of radio frequency waves. At 100 cm above the snow surface, they installed four transceiver dipole antennas built using an Arduino Mini Board, one of which served as a source node and the other three as destination nodes, all of which were located in a far-field area from the source node [10]. The measurements were conducted at one-minute intervals throughout the snowfall for 11.5 hours. Upon the conclusion of the measurement period, a cumulative snow accumulation of 60 cm had accumulated above the node level. Based on the recorded received signal strength indicator (RSSI) data, it is suggested that the PL of the channel may be accurately characterized by 3rd-order polynomial models, as long as the nodes are not buried in the snow [10]. When the nodes are covered with snow, the PL may be described using the exponential model. The more nodes are covered with snow, the more closely the PL growth follows the exponential model [10]. Javali et al. have carried out a similar experiment campaign, examining near-ground Wireless Sensor Network (WSNs) PL in snow-covered forest areas at 2.45 GHz center frequency with 60 cm snow thickness [11]. Their results confirm that for no snow conditions, the sensible signal range increases and the PL grows gradually, whereas the PL shows exponential growth in the presence of snow. The results also revealed that two-slope log-distance models provide the best fit for the outdoor forested PL in both snow and non-snow conditions [11]. Another work by Nakamura et al. used several snow plates with varying thicknesses between transmitter and receiver horn antennas to investigate the effect of snow accretion on antenna radome on receiver power at 45 GHz at varied snow moisture contents (5.5%, 10%, and 14.6%) [12]. The results indicate that the moisture in the snow on the antenna's surface causes a significant reduction in receiver power of up to 45 dB [12]. In a very recent study, Abdulali and Salous [13] examined snowfall attenuation at 25.84 GHz and 77.54 GHz bands over direct 36 m and 200 m fixed links using fixed polarizations. They measured signal levels during clear weather to use them as a reference baseline for comparison. They also measured the snowfall rate periodically using the PWS100 Weather Sensor station and recorded the signal levels during snowfall at the same time frame. The snow attenuation levels were derived from the difference between the reference signal level and signal levels during snowfall. They have come with attenuation plots as a function of the snowfall rate. The findings suggest that the snow attenuation grows with the increase in snow intensity, following the snowfall trend. Also, they imply that snow attenuation is proportional to separation distance. Moreover, they claim that cross-polarized links suffer larger attenuation than co-polarized ones [13].

Previous studies have investigated how environmental factors such as rain, snow, and fog influence mmWave propagation; however, the effects of snowstorms, particularly in outdoor environments, have not been thoroughly examined and modeled yet. Though their findings are closely related to the influence of snowfall on mmWave channels, particularly authors of [13] have given insufficient focus to the behavior of the PL of mmWave channels depending on T-R separation and its parameters. Seeing that PL modeling is vital for network planners to design resilient and high-coverage mmWave systems in snowstorm environments, much remains to be explored. Snowstorm conditions present different challenges, such as quick snow accumulation, increased moisture levels, and powerful winds, which greatly influence signal attenuation and PL parameters. The lack of clarity in this area restricts the effective design, deployment, and coverage of robust mmWave communication systems in areas prone to severe winter conditions. Therefore, understanding and managing the snowstorm effect on PL is significant in

designing robust mmWave cellular networks in snow-covered areas. By experimentally investigating the 60 GHz mmWave channel under snowstorm conditions, this work addresses the challenges mentioned above and provides meaningful advancements.

Our study intends to isolate and quantify the impact of harsh weather atmospheric factors on the attenuation of the 60 GHz mmWave signal. Snow density, humidity, and high wind speed are the primary contributors to mmWave signal attenuation. Since, in a long-term sense, these dominant factors are spatially consistent over the transmitter-receiver separation and do not exhibit rapid temporal variations, they can be cumulatively quantified using large-scale fading. In addition, because of the stationary aspects of our setup and a clear LOS, the rapid temporal environmental PL variations due to terminal movement and other time-varying changes can be treated as negligible. Therefore, this study mainly focuses on large-scale fading while neglecting small-scale fading effects. Also, an important extension of 60 GHz studies could be to consider the influence of Doppler-induced frequency shifts for vehicular communication systems. However, our stationary setup can closely mirror real-world point-to-point backhaul links and hence can be solely important in communication systems for infrastructures having base stations or relay points. To do so, this work extends the well-known Close-In Free Space reference distance (CI) path-loss model to account for snowstorm-specific factors such as snowflake scattering, atmospheric absorption, and wind-driven dynamics inherent to the Northern Central Asia climate. By analyzing received power at varying transmitter-receiver distances, we quantify the impact of snowstorms on PL and propose modifications to the CI path-loss equation. In this regard, the primary focus of the paper is on experimentally deriving the PL parameters like Path-loss Exponent (PLE) and Standard Deviation of the Shadow Fading (SF) factor inherent to indoors, i.e., lab environment, and outdoors under snowstorms in 60 GHz band. The study uses the CI model to estimate the PLE and SF standard deviation. Since traditional free-space models are assumed to have a minimal environmental impact, integration of exponential and polynomial modifications into the CI model can offer more accurate PL predicting under snowstorm conditions. Therefore, this work examines how accurately the exponential and polynomial functions can describe the PL of the 60 GHz mmWave channel under outdoor snowstorm conditions. We use the R^2 test to assess the accuracy of fitting the 2nd-order polynomial and single and two-term exponential functions to the experimental PL data. We also derive modifying terms to the considered CI PL model using the respective exponential and polynomial functions by exploiting the discrepancy between theoretical and experimental data. Accordingly, we propose modified PL equations that account for snowstorm-induced factors, offering more accurate predictions of PL behavior under snowstorm conditions. Finally, the R^2 test is also employed to evaluate the accuracy of the modified PL equations. Altogether, our work contributes to the field by providing insights into how snowstorm conditions expressed by snowflake scattering, moisture absorption, and strong dynamic wind effects influence the 60 GHz mmWave signal propagation. In addition, it offers modified PL equations for optimization of 60 GHz mmWave network performance in harsh climates inherent to regions of Northern Central Asia and other regions with similar characteristics.

The paper is organized as follows. Section II provides a summary of the existing measurement campaigns in mmWave bands and beyond, emphasizing their methodologies, findings, and limitations. Section III describes the experimental hardware setup and the experiment regulations and provides an analytical definition of the CI PL model used to obtain the relevant PL parameters. The R^2 metric description is also introduced. In Section IV, we present the determined PL parameters inherent to the indoor and outdoor snowstorm environments. Here, we also present the results of the exponential and polynomial fits to the experimental PL data and CI model modifications. The research contributions, limitations, and future work are also discussed. Finally, Section V concludes the paper.

II. RELATED WORK

The behavior of mmWave signal transmission has been studied in diverse scenarios, including regions with foliage, indoor office settings, and various weather conditions.

Lai et al. [14] performed a comprehensive study utilizing Ansys HFSS SBR+ ray tracing simulator, which was calibrated against channel measurements at 60 GHz. Seven trees were digitally modeled as intricate meshes of leaves and branches, ensuring an accurate representation of foliage characteristics. Measurements used the Terragraph double-directional channel sounder throughout the summer and winter seasons, encompassing 14 transmitter-receiver (T-R) locations per tree and exceeding 573,000 channel scans. The precise configuration allowed the authors to measure the loss of penetration of the foliage, which amounted to 40 dB per tree. Significant seasonal differences were observed, with angular spreads notably wider in summer attributed to denser foliage. The findings underscored the significant influence of seasonal variations on path loss and multipath propagation, indicating the need for accurate foliage modeling in outdoor network design. The study's limitations included a focus on stationary foliage in controlled environments and neglecting dynamic weather conditions such as snowstorms or high-speed winds, which are crucial for the design of robust communication systems in adverse climates.

In another study, using deciduous trees and a variety of weather conditions including ice and snow, Zavorka et al. [15] aimed to characterize the 80 GHz channel in outdoor settings. Their approach included using a channel sounder to collect channel impulse response (CIR) data, which were then analyzed for characteristics including path loss, Rician K-factor, root mean square (RMS) delay spread, and more. Compared to naked trees, trees with

foliage had an attenuation of 2.16 dB/m greater, according to the study. The properties of multipath propagation were altered due to the increased absorption and reduced snow and ice scattering effects. These findings demonstrated that stationary environmental conditions significantly affect mmWave signals. Nevertheless, the research did not account for more complicated and dynamic weather conditions, such as metropolitan areas with strong winds or high snowfall rates since it only looked at static scenarios and one deciduous tree in a controlled setting.

Recent studies have examined indoor mmWave propagation and its dependence on settings. The extensive indoor tests at 60 GHz were carried out by Wu et al. [16] in an office setting of 7.2 × 7.2 × 3 m. To study both LOS and NLOS scenarios, authors used directional antennas and uniform virtual arrays (UVAs). To provide estimates for high-resolution characteristics such as power, delay, and azimuth-elevation angles of multipath components, the Saleh-Valenzuela (S-V) model and the SAGE method were used. Delay dispersion was affected by room size, wall materials, and antenna polarization, whereas azimuth angular spreads were found to be far greater than elevation spreads. Though the use of specific directional antennas and UVAs may introduce biases related to the equipment's characteristics, this work still sheds light on indoor mmWave system design.

In a conference room, Kim et al. [17] used a high-resolution frequency-domain channel sounder to study the propagation of signals at 60 GHz and 300 GHz. To verify their findings, the authors used ray-tracing simulations to examine angular spreads and delay spreads on azimuth and elevation planes. Both frequencies were also evaluated using large-scale parameters (LSPs). At 300 GHz, LOS propagation was found to be more dominant because multipath components were attenuated more. As a result of less multipath richness at higher frequencies, the angular and delay spreads were smaller at 300 GHz compared to 60 GHz. The study overlooks the effects of human mobility and object displacement, which are prevalent in dynamic circumstances, and instead concentrates on a static indoor conference room scenario. However, the paper generally offers a comprehensive study of important large-scale factors such as angle spreads and delay spreads, which are fundamental for the design of mmWave indoor communication systems.

Recent research highlighted snow-induced attenuation in communication systems on mmWave and THz frequencies. Snow-induced attenuation was investigated by Amaya et al. [18] on a satellite link operating at 20.2 GHz (Ka-band) using beacon signals from the Anik F2 satellite. Conducted over two years in Ottawa, Canada, this study analyzed the impact of snow, rain, and mixed precipitation on signal attenuation along slant paths. The results showed that snow attenuation at 20.2 GHz was modest, rarely exceeding 2 dB, with wet snow contributing more significantly than dry snow. Although valuable insights into frequency-dependent attenuation for satellite links can be inferred from this study, it focuses on slant-path propagation and does not address the specific challenges faced by terrestrial mmWave networks at higher frequencies.

A decent attention was recently drawn to snowflakes' molecular absorption and scattering effects on THz waves. The authors of [19] suggest that in the THz band, snow-induced attenuation is mainly attributed to scattering effects due to a decrease in water content. The effects of snowflake scattering can be explained using Mie scattering theory since the diameter of the snowflakes is extensively larger than 0.03 times the wavelength of a THz signal [20]. THz frequencies experience significantly higher scattering since, based on Mie scattering theory, the larger the ratio of the particle's diameter to the wavelength, the stronger the scattering intensity and hence stronger the attenuation. THz signals experience much stronger scattering and attenuation, as snowflake sizes (1–5 mm) are significantly larger relative to the shorter wavelengths of THz frequencies. In general, extreme sensitivity to humidity at a molecular level and the significantly higher scattering intensity due to its shorter wavelength make the THz band less suitable for snowstorm environments. However, mmWave bands can balance higher capacity with manageable attenuation in snowstorm settings. Moreover, the need for greater focus on mmWave frequencies can also be motivated by their practical deployment in emerging outdoor communication systems, as mmWave technologies are already at the forefront of commercial adoption.

These investigations collectively illustrate substantial efforts to define the propagation of mmWave under various scenarios. However, a significant gap still prevails in comprehending the impacts of dynamic weather conditions, especially snowstorms, on 60 GHz mmWave propagation. This work addresses the mentioned gaps by investigating outdoor snowstorm scenarios, measuring their effects on path loss and received power, and suggesting modifications to the path-loss model to improve the robustness of mmWave communication systems in challenging weather conditions.

III. METHODOLOGY

A. MmWAVE HARDWARE SYSTEM SETUP

Fig. 1 shows the setup used to investigate the mmWave spectrum at the 60GHz frequency. The system design employs identical transceivers for both the receiver and transmitter sides. Each transceiver is made up of the Voltage Controlled Oscillator (VCO), I/Q Mixer, and Horn Antenna. Fig. 2 illustrates the detailed close-up of the transceiver components of the 60 GHz mmWave channel system including the horn antenna, VCO, and I/Q mixer. Table 1 summarizes the system specs for the 60 GHz mmWave technology. In the transceiver, the VCO generates a 60 GHz continuous wave carrier signal, which is directly transmitted without modulation, as no baseband signal is used in the experiment. Our PL experiments focus solely on the power characteristics of 60 GHz mmWave signal propagation. Therefore, the I/Q mixer is not used to mix the VCO signal with a baseband signal; instead, it forwards the unmodulated VCO signal,

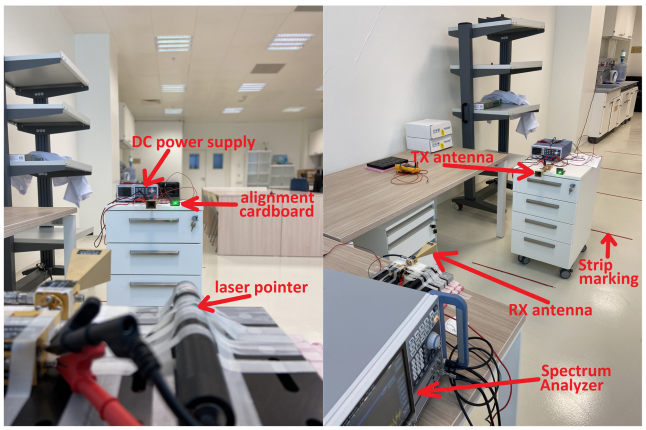

FIGURE 1. Path-loss indoor experiment setting for 60 GHz mmWave channel.

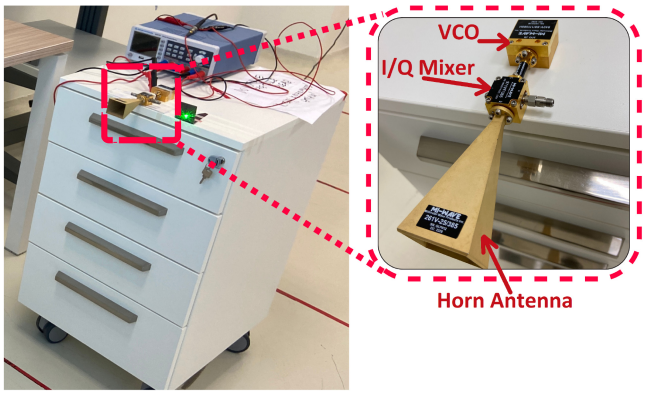

FIGURE 2. Close-Up of Transceiver Components (Horn Antenna, Voltage Controlled Oscillator, and I/Q Mixer) for 60 GHz mmWave channel.

resulting in some internal conversion losses as detailed in Table 1. Subsequently, the signal is transmitted out using the horn antenna, which ensures effective signal propagation due to its narrow half-power beamwidth (HPBW) of 9° in the E-plane and 10° in the H-plane and its high directional gain of 25 dBi.

On the receiver side, the same components are used to perform down-conversion. The horn antenna captures the incoming 60 GHz signal, which is then directed to the I/Q mixer. Here, the VCO signal is used to down-convert the received RF signal to an intermediate frequency. The resulting signal from the in-phase port of the I/Q mixer is fed to the spectrum analyzer for analysis.

According to the system specs, the VCO frequency can be tuned from 59 to 61 GHz depending on a DC control voltage range of 8 to 10 volts. While applying a 9 V control voltage to both VCOs from the same output channel of the DC power supply (to generate a 60 GHz carrier signal at TX and down-convert in at RX), the spectrum analyzer at the RX site detected an intermediate signal with a frequency of 800-900 MHz. This factory miscalibration of two transceivers allowed us to observe a receiver signal without the need to transmit a modulated baseband signal by mixing it with the

TABLE 1. System specifications for 60 GHz channel measurement.

Equipment	Features
VCO	Carrier frequency 60 GHz Bandwidth 2 GHz Waveguide loss 0.02 dB Control voltage 8-10 V Power output 17 dBm
I/Q Mixer	LO-to-RF isolation loss 28 dB RF-to-IF conversion loss 10 dB
TX power	3.98 dBm (see (1))
TX Antenna	Gain 25 dBi 9° E-plane HPBW 10° H-plane HPBW Linearly polarized
RX Antenna	Gain 25 dBi 9° E-plane HPBW 10° H-plane HPBW Linearly polarized
The spectrum analyzer	Frequency range: 2 Hz−43.5 GHz Max. analysis bandwidth: 8312 MHz Pre-amplification: 30 dB

60 GHz carrier signal from the VCO. The precise level of the bias voltage of 6V applied to both VCOs was maintained throughout the experiment to minimize instrumental error. Moreover, a rechargeable monochromatic green laser pointer on the RX side ensured systematic error minimization and proper surface-to-surface LOS alignment. It is positioned at the same distance from the center of the RX antenna as the alignment cardboard is from the center of the TX antenna (see Fig. 1).

In indoor and outdoor experiments, the receiver side remained stationary while the transmitter system moved away. The TX power is the signal transmission power, computed by subtracting the conversion losses of the Waveguide, Local Oscillator to Radio Frequency wave (LO-to-RF), and of the Radio Frequency wave to Intermediate Frequency wave (RF-to-IF) from the VCO power output and adding the TX antenna gain. The transmitter power is 3.98 dBm and is calculated as follows:

$$P_{\mathrm{TX}} = P_{\mathrm{VCO}} - (L_{\mathrm{WG}} + L_{\mathrm{RF2IF}} + L_{\mathrm{LO2RF}}) + G_{\mathrm{TX}}, \quad (1)$$

where P_{VCO} is the VCO power output, L_{WG} is the waveguide loss, L_{RF2IF} and L_{LO2RF} are the RF-to-IF and LO-to-RF conversion losses specific to the I/Q Mixer, respectively (see Table 1). In accordance with Table 1, the receiver power is defined as follows:

$$P_{\mathrm{RX}} = P_{\mathrm{O}} + L_{\mathrm{RF2IF}} + L_{\mathrm{LO2RF}} + L_{\mathrm{W}} - G_{\mathrm{RX}} - 30, \quad (2)$$

where P_{O} is the received power observed on the spectrum analyzer, 30 dB is a pre-amplification by the spectrum analyzer, L_{W} is losses associated with wires and connectors between the receiver system and the spectrum analyzer, which is around 9.34 dB and G_{RX} is the receiver antenna gain (see Table 1). The L_{W} loss is found by

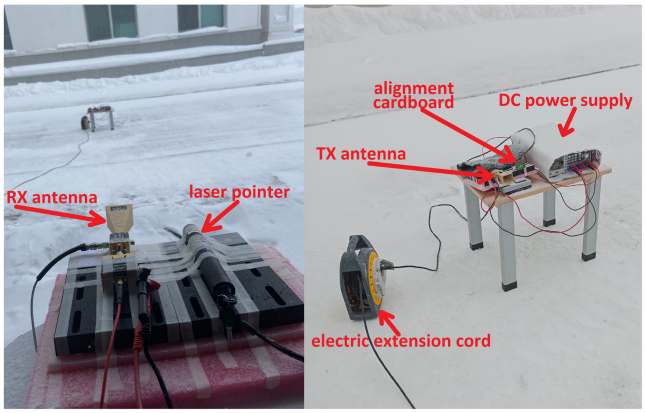

FIGURE 3. Path-loss outdoor experiment setting for 60 GHz mmWave channel under snowstorm.

summing the losses of the respective high-frequency RF cables and connector adapters according to their datasheets. The observed power is adjusted by subtracting the pre-amplification provided by the spectrum analyzer and the receiver antenna gain because the actual receiver power is affected by both amplifications. Similarly, the purpose of adding the L_{RF2IF}, L_{LO2RF} conversion losses and the L_{W} loss is to compensate them for determining the actual receiver power at the receiver antenna. This is necessary because accurately defining the PL requires determining the actual powers of the receiver and transmitter.

B. MEASUREMENT SCOPES

Both indoor and outdoor measurements (Fig. 1) are done exclusively in a Far Field region, out of the Fresnel Region to ensure the minimal inductive effect and accurate RX power. An agreed near-field region can be defined by:

$$r \leq \frac{2D^2}{\lambda}, \tag{3}$$

where D is the largest linear dimension of the Horn antenna, $\lambda = c/f$ is the wavelength corresponding to the 60 GHz band, c is the speed of light and f is the frequency. According to the outline drawing specifications of the horn antenna [21], D is 4.328 cm, hence the Fresnel Region is $r \leq 0.75m$ according to (3). Given that the Far-Field area is next to the Fresnel Region, the antenna waves are expected to transition into the Far-Field region beyond a distance of 75 cm, resulting in stability of the field's inductive effects.

As shown in Fig. 1, the receiver system remains fixed at the 0 mark (floor strip markings) in this setup, while the transmitter system moves away, ranging from 1 m to 10 m T-R distance. During indoor experiments, 10 received power measurements are taken at each integer meter interval of the T-R distance. In contrast, outdoor experiments (Fig. 3) cover 8 integer distance measurements, with measurements at the 4th and 6th meters excluded. These exclusions were made to shorten the duration of the experiment and minimize the risk of equipment damage due to cold weather. To further reduce the cold-weather damage, all equipment, including the spectrum analyzer and DC power supplies, was coated with polyurethane foam with an outer layer of polypropylene aluminum foil for thermal insulation. The outdoor experiments were conducted on the Nazarbayev University (NU) campus on February 8, 2024, at 1:00 p.m. local time in Astana, Kazakhstan. The experiment's climatic characteristics comprised a temperature of −9°C, relative humidity of 88%, atmospheric pressure of 1009.8 millibars, 0.2 mm/h snowfall rate, and a wind speed of 18 meters per second. These values align with typical high wind-speed snowstorm conditions inherent to Astana and other Northern Central Asia regions [22]. Indoor measurements are limited to a maximum of 10 meters due to limited laboratory space. In contrast, such a limit in the harsh outdoor environment is primarily determined by strong PL, which causes the observed power at a 10 m T-R distance to be significantly low, almost imperceptible, i.e., close to background noise.

In both indoor and outdoor scenarios, measurements are taken by moving away the transmitter system to an integer-meter T-R distance from the receiver system. Before each measurement, perfect surface-to-surface alignment of the transmitter and receiver antennas was established using the laser pointer to ensure the ideal LOS condition, while minimizing systematic error. In both experiments, at least ten observed receiver power values were recorded for each T-R separation distance. The PL per distance and measurement, and for both indoor and outdoor conditions, can be described as:

$$PL = P_{\text{TX}} - P_{\text{RX}}. \tag{4}$$

C. PATH-LOSS MODELLING

The 60GHz mmWave channel Path-loss in both indoor and outdoor contexts is modeled using the close-in free space reference distance (CI) model due to its high accuracy and its ability to validate other models [23]. For the carrier frequency f, denoted by (5), the free space Path-loss (FSPL, 1 m) is the decibel (dB) measurement at a 3D T-R separation distance of 1 meter:

$$\text{FSPL}(f, 1m)[\text{dB}] = 10\log_{10}\left(\frac{4\pi f}{c}\right)^2, \tag{5}$$

where c is the speed of light. The CI model utilizes a reference distance of 1 meter, and it can be expressed as:

$$\text{PL}^{\text{CI}}(f, d)[\text{dB}] = \text{FSPL}(f, d_0) + 10n\log_{10}\left(\frac{d}{d_0}\right) + X_\sigma^{\text{CI}}. \tag{6}$$

Here, n is the Path-loss exponent (PLE), d is the 3D T-R separation distance and X_σ^{CI} is a random variable (RV) called Shadow Fading (SF) factor, which defines large-scale channel inconsistency as a zero-mean Gaussian random variable with standard deviation σ. The SF RV can be expressed as:

$$\begin{aligned} X_\sigma^{\text{CI}} &= \text{PL}^{\text{CI}}(f, d)[\text{dB}] - \text{FSPL}(f, 1\text{ m})[\text{dB}] - 10n\log_{10}(d) \\ &= A - nB, \end{aligned} \tag{7}$$

where A (in dB) suggests $\mathrm{PL}^{\mathrm{CI}}(f,d)[\mathrm{dB}] - \mathrm{FSPL}(f,1\ \mathrm{m})[\mathrm{dB}]$ and B indicates $10n\log_{10}(d)$. The Minimum Mean Square Error (MMSE) method is employed to estimate the SF standard deviation and PLE parameters from experiment data to model indoor and Astana's outdoor 60GHz mmWave channel using the CI model [23]. Applying the MMSE method on (7), the standard deviation σ^{CI} of the X_σ^{CI} RV can be found according to [23] as follows:

$$\sigma^{\mathrm{CI}} = \sqrt{\sum X_\sigma^{\mathrm{CI}2}/N} = \sqrt{\sum (A - nB)^2/N}, \tag{8}$$

where N denotes the number of measured PL data points. With the sums calculated straight from the individual elements, the summations encompass the whole sample size. The constituents are added directly for these sums since they are all represented in dB. The σ^{CI} term may be minimized by equating its derivative with respect to n to zero:

$$\begin{aligned}\frac{d\sum (A-nB)^2}{dn} &= \sum 2B(nB-A)\\ &= 2\sum B(nB-A)\\ &= 2\left(n\sum B^2 - \sum BA\right) = 0.\end{aligned} \tag{9}$$

Therefore, the expression in (9) yields n as:

$$n = \frac{\sum BA}{\sum B^2}. \tag{10}$$

Thus, the CI model's minimum σ^{CI} is:

$$\sigma_{\min}^{\mathrm{CI}} = \sqrt{\sum \left(A - B\frac{\sum BA}{\sum B^2}\right)^2/N}. \tag{11}$$

The closed-form solutions for n and σ^{CI}, to make A and B terms suitable for MATLAB processing, can be denoted as column vectors [23]. In matrix form, n can be expressed as:

$$n = A^T\left(B^TB\right)^{-1}B. \tag{12}$$

Similarly, the closed-form solution of σ^{CI} is as follows:

$$\sigma_{\min}^{\mathrm{CI}} = \sqrt{\sum \left(A - (A^T(B^TB)^{-1}B)B\right)^2/N}. \tag{13}$$

D. SNOWSTORM PL DATA FIT ESTIMATION METRIC

As was noted earlier, snowstorms can affect the attenuation patterns of RF waves [10]. Estimating how the snowstorm PL data fits the exponential function is hence of present interest. The data has been fitted into exponential functions with one term and with two terms. For the sake of comparison, it is also fitted into 2nd order polynomial function. To estimate the goodness of fit, the R^2 test is employed and is defined utilizing the ratio of the sum of squares of regression (SSR), i.e., residuals, to the total sum of squares (TSS):

$$R^2 = 1 - \frac{SSR}{TSS}, \tag{14}$$

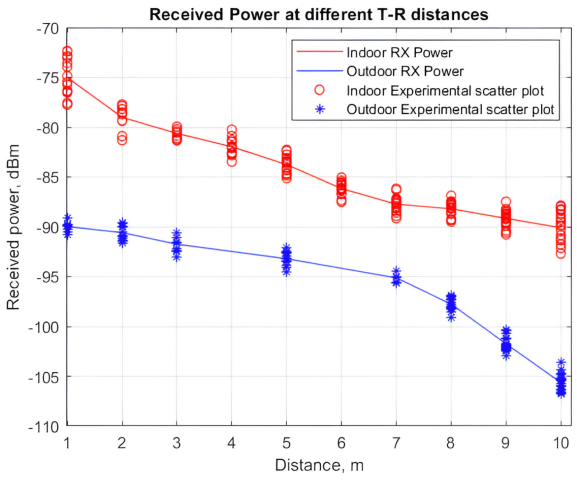

FIGURE 4. Measured receiver power at indoor and outdoor snowstorm scenarios with 3.98 dBm transmit power at 60 GHz.

where $SSR = \sum_{i=1}^{n}(\widehat{y}_i - \bar{y})^2$, $TSS = \sum_{i=1}^{n}(y_i - \widehat{y}_i)^2$, y_i's are the experimental PL data, $\bar{y}$ is the mean of y_i's and $\widehat{y}_i$'s are the predicted values by the considered function. We used the R^2 metric since it is a well-recognized and intuitive criterion for assessing the model's quality of fit. R^2 is a useful metric for comparing how accurately various mathematical models represent the snowstorm PL data because it specifically measures a proportion of variance in the observed data that can be explained by the fitted model. The R^2 statistic measures the extent to which an independent variable, i.e., fitted function, can predict or explain variation in a dependent variable based on experimental PL data. The range of the metric is 0 to 1. The model explains or predicts 0% of the association between the dependent and independent variables with an R^2 value of 0, whereas it refers to 100% prediction with 1.

IV. RESULTS

A. PL PARAMETERS

This subsection provides the experimental findings for the 60 GHz mmWave channels indoors and outdoors. Fig. 4 shows the receiver power plots measured indoors and outdoors. The outdoor plot (blue plot) shows a steeper fall in receiver power beyond 7 meters, suggesting a different attenuation behavior than the indoor scenario (red plot). Both plots are built using the mean values of scattered receiver readings per T-R distance. The PL plots are constructed by fitting the observations to the CI model by defining the parameters A and B shown in (7), thereby solving for PLE and $\sigma_{\min}^{\mathrm{CI}}$ via (12) and (13). Table 2 shows the parameters of the PLE and SF standard deviation for both cases. The outdoor PLE is 1.5 times that of the indoor PLE, indicating stronger attenuation during snowstorms. Thus, as a controlled baseline, indoor measurements can aid in isolating and highlighting snowfall impacts on mmWave propagation.

Fig. 5 shows indoor and outdoor PL plots. The PL values for both cases are calculated using (4). Experimental PL

TABLE 2. PLE and $\sigma^{\text{CI}}_{\text{min}}$ parameters.

Scenario	PLE	σ^{CI}, dB
Indoor	2.77	4.05
Outdoor	4.12	9.32

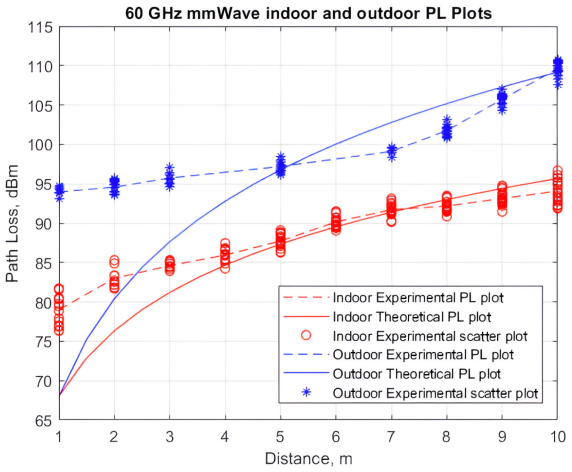

FIGURE 5. mmWave experimental and theoretical PL plots for indoor and outdoor snowstorm scenarios using the obtained parameters of $PLE = 2.77$, $\sigma^{\text{CI}} = 4.05dB$ and $PLE = 4.12$, $\sigma^{\text{CI}} = 9.32dB$, respectively.

graphs reveal a loss of around 15 dB in the snowstorm compared to the indoor environment at a 1 m T-R separation. This gap has dropped by almost half at the 7 m T-R distance before increasing again beyond that. Finally, the divergence has returned to 15 dB at a 10 m T-R distance. Theoretical PL plots for indoor and outdoor settings start with closer PL values and diverge as the T-R distance increases. The MMSE approach expressed in (12) yielded PLE values of 2.77 and 4.12 for indoor and outdoor settings, respectively (see Table 2). Furthermore, the MMSE-based expression in (13) likewise yielded standard deviation values of 4.05 dB and 9.32 dB of the SF parameter, i.e., $\sigma^{\text{CI}}_{\text{min}}$, for indoor and outdoor settings (see Table 2). Indoor and outdoor PLE levels are in the acceptable range between 2 and 5. Both of the data in Fig. 5 mostly indicate that PL increases with T-R separation.

The indoor environment presented a controlled setup with LOS conditions. Faced with office barriers and reflections, the vulnerable mmWave signal undergoes losses, which may explain a reasonably fast signal attenuation of 2.77. These values are in line with regular indoor surroundings, where reflections and multipath propagation due to walls and furniture prevail. Hence, the PL observed at short T-R distances is primarily due to the vulnerability of mmWave channels before multipath effects. Reflections from walls and other objects provide destructive interference in a restricted indoor area, consequently degrading the signal. The losses are further degraded due to the amplification of the sensitivity to orientation mismatches of the linearly polarized horn antennas. These findings are consistent with the observations provided by Wu et al. [16], who reported similar patterns in office environments.

The outdoor PLE of 4.12 suggests a higher attenuation rate in outdoor open spaces, especially during snowstorms. Since the power of outdoor signal is more variable and unpredictable due to irregularities of terrain and environmental factors such as snowflakes, buildings, and high wind speed, the $\sigma^{\text{CI}}_{\text{min}}$ of 9.32 dB is higher than the indoor $\sigma^{\text{CI}}_{\text{min}}$ of 4.05 dB. At a 1-meter T-R distance, snowstorm PL graphs show 15 dB more loss than indoors. The difference halves when the T-R distance reaches 7 meters, then rises back again at 10 meters. The behavior of outdoor wireless channel behavior at 60 GHz mmWave frequencies has been considerably attenuated by several factors. The 88% relative humidity signals considerable atmospheric moisture, which can impede signal transmission by absorption and scattering [24]. Snowstorms can weaken mmWave transmissions due to air moisture. In addition, cold weather can increase air moisture and signal absorption, increasing signal attenuation [24]. Furthermore, snowflakes act as scatterers, especially at 60 GHz where the signal wavelength becomes comparable to their size ranging between 2-5 mm as assessed visually. In addition, atmospheric absorption increases because of the high relative humidity. High wind speeds of 18 m/s allow snowflakes to drift randomly and rapidly, further boosting snow density naturally and creating variability in the signal path through snowflake dynamics. Therefore, as previously mentioned, greater snow intensity increases mmWave signal attenuation according to [13]. The results of [10] may explain the shift in outdoor PL to an exponential pattern once the distance between the transmitter and receiver exceeds 7 meters. It can be linked to the increase in the density of snowflakes due to strong winds, thereby blocking the signal more strongly, as the transmitter moves further away from the receiver. In addition, the accumulation of snow on the antenna's surface can contribute to the increasing PL, as confirmed by [12], since more snow had been building up on both antennas over time during the experiment.

B. SNOWSTORM PL DATA FITTING

Fig. 6 illustrates the fit plots of the F_1, F_2 and F_3 functions, which represent the exponential function with a single term, exponential function with 2 terms and the 2nd-order polynomial function, respectively.

The obtained functions of the distance of the fit plots are as follows:

$$\text{F}_1(d)[\text{dB}] = 90.62e^{0.01693d}, \tag{15}$$

$$\text{F}_2(d)[\text{dB}] = 93.49e^{0.003276d} + 0.2663e^{0.3903d}, \tag{16}$$

$$\text{F}_3(d)[\text{dB}] = 0.2457d^2 - 1.118d + 95.8. \tag{17}$$

The $R^2 = 0.8936$ is the highest R^2 value and is obtained for the $F_2(d)$ approximation of the PL. For the $F_3(d)$ and $F_1(d)$ functions, the R^2 showings are 0.9716 and 0.8936, respectively. The higher-order polynomials have not been examined, since using them results in over-fitting the

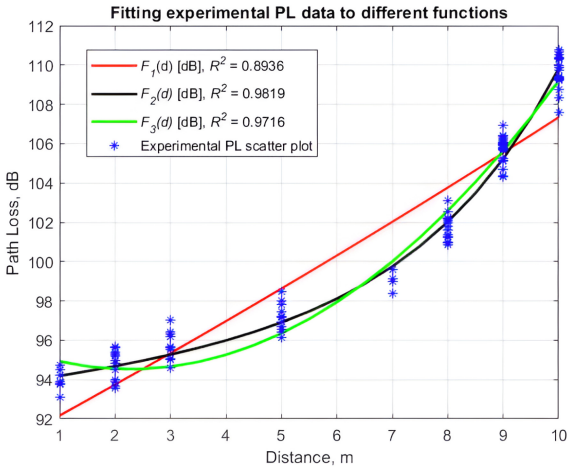

FIGURE 6. Fitting experimental PL data to different functions.

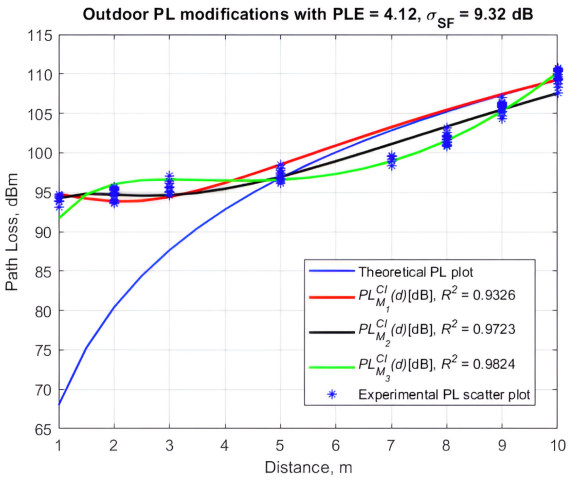

FIGURE 7. Modified outdoor PL with $PLE = 4.12$, $\sigma^{CI} = 9.32dB$.

available PL data, as the snowstorm experiment is conducted only once. Generally, the two-term exponential function is a fair approximation of the PL behavior for the 60 GHz mmWave channel during snowstorms. Moreover, this aligns with the earlier mentioned results by [11] which reveal the best fit is obtained by the two-slope log-distance models for the outdoor PL in both snow and non-snow conditions.

C. SNOWSTORM PL EQUATION MODIFICATION

Exponential and polynomial functions used in deriving $F_1(d)$, $F_2(d)$ and $F_3(d)$ can also be used to update the PL equation for snowstorms in the 60 GHz mmWave channel by modifying the expression in (6). The theoretical PL plot in Fig. 5 is subtracted from the experimental PL data to obtain the discrepancy data. The discrepancy data are then fitted into the exponential functions with one and two terms and the 2nd-order polynomial function to obtain modifying terms, namely (21), (22) and (23). Finally, the modifying terms are compensated to the initial CI PL model expression in (6) to develop the updated snowstorm-specific PL equations in the 60 GHz band. The updated PL equations are as follows:

$$\mathrm{PL}^{\mathrm{CI}}_{\mathrm{M}_1}(f,d)[\mathrm{dB}] = \mathrm{PL}^{\mathrm{CI}}(f,d)[\mathrm{dB}] + \mathrm{M}_1(d)[\mathrm{dB}], \quad (18)$$

$$\mathrm{PL}^{\mathrm{CI}}_{\mathrm{M}_2}(f,d)[\mathrm{dB}] = \mathrm{PL}^{\mathrm{CI}}(f,d)[\mathrm{dB}] + \mathrm{M}_2(d)[\mathrm{dB}], \quad (19)$$

$$\mathrm{PL}^{\mathrm{CI}}_{\mathrm{M}_3}(f,d)[\mathrm{dB}] = \mathrm{PL}^{\mathrm{CI}}(f,d)[\mathrm{dB}] + \mathrm{M}_3(d)[\mathrm{dB}], \quad (20)$$

where $\mathrm{M}_1(d)$[dB], $\mathrm{M}_2(d)$[dB] and $\mathrm{M}_3(d)$[dB] are the modifying terms, representing the exponential function with a single term, exponential function with 2 terms and the 2nd-order polynomial function, respectively. The $\mathrm{M}_1(d)$[dB], $\mathrm{M}_2(d)$[dB] and $\mathrm{M}_3(d)$[dB] are computed as:

$$\mathrm{M}_1(d)[\mathrm{dB}] = 53.3041e^{-0.6901d}, \quad (21)$$

$$\mathrm{M}_2(d)[\mathrm{dB}] = -1166464e^{-0.3272d} + 1166509e^{-0.3273d}, \quad (22)$$

$$\mathrm{M}_3(d)[\mathrm{dB}] = 0.6909d^2 - 10.1245d + 33.1132. \quad (23)$$

The PL plots with modifications, namely $\mathrm{PL}^{\mathrm{CI}}_{\mathrm{M}_1}(f,d)$[dB], $\mathrm{PL}^{\mathrm{CI}}_{\mathrm{M}_2}(f,d)$[dB] and $\mathrm{PL}^{\mathrm{CI}}_{\mathrm{M}_3}(f,d)$[dB], along with the original theoretical PL plot are shown in Fig. 7. Although the two-term exponential function $\mathrm{F}_2(d)$[dB] has the highest R^2 when fitting the experimental data, now the best fit for the discrepancy data (between theoretical and experimental PL) is achieved by the $\mathrm{M}_3(d)$[dB], i.e., 2nd order polynomial modification with $R^2 = 0.9824$. The two-term exponential modification $\mathrm{M}_2(d)$[dB] also accurately describes the discrepancy data, with $R^2 = 0.9723$. Moreover, $\mathrm{M}_1(d)$[dB] has the least R^2 value of 0.9326. The notable difference in R^2 values between the $\mathrm{M}_1(d)$[dB] and $\mathrm{M}_2(d)$[dB] or between $\mathrm{F}_1(d)$[dB] and $\mathrm{F}_2(d)$[dB] is presumably due to the existence of two decay modes in the discrepancy data or the presence of two exponential growth modes in the PL data, respectively. The proposed modifications to the CI PL model ($\mathrm{M}_1(d)$[dB], $\mathrm{M}_2(d)$[dB] and $\mathrm{M}_3(d)$[dB]) can offer distinct benefits and practical applications. The single-term exponential modification $\mathrm{M}_1(d)$[dB] offers a simple representation of snowstorm PL at 60 GHz, making it computationally efficient when quick approximations are needed. It can be handy in early-stage network design or feasibility studies when precision is secondary to simplicity. Meanwhile, the two-term exponential modification $\mathrm{M}_2(d)$[dB] can capture more complex snowstorm PL patterns with higher accuracy. Thus, $\mathrm{M}_2(d)$[dB] modification would suit best for applications requiring detailed modeling, including fine-tuning link budgets or optimizing dense mmWave deployments. Finally, the second-order polynomial model $\mathrm{M}_3(d)$[dB], while achieving the highest R^2, requires cautious application due to the potential risk of over-fitting. This model suits scenarios where experimental circumstances closely align with the deployment environment. Overall, these results suggest that snowstorm-specific factors such as snowflake dynamics and moisture of the antenna surface introduce complex attenuation patterns that deviate from the standard CI model. This work proposes the modified equations of

the CI PL model (24), (25), and (26) to account for these discrepancies and provide improved accuracy for predicting signal behavior in snowstorm conditions. These equations can be presented in the following general form:

$$\mathrm{PL}_{\mathrm{E}_1}^{\mathrm{CI}}(f,d)[\mathrm{dB}] = \mathrm{PL}^{\mathrm{CI}}(f,d)[\mathrm{dB}] + Ae^{Bd}, \quad (24)$$

$$\mathrm{PL}_{\mathrm{E}_2}^{\mathrm{CI}}(f,d)[\mathrm{dB}] = \mathrm{PL}^{\mathrm{CI}}(f,d)[\mathrm{dB}] + Ae^{Bd} + Ce^{Dd}, \quad (25)$$

$$\mathrm{PL}_{\mathrm{P}_2}^{\mathrm{CI}}(f,d)[\mathrm{dB}] = \mathrm{PL}^{\mathrm{CI}}(f,d)[\mathrm{dB}] + Ad^2 + Bd + C, \quad (26)$$

where $PL_{\mathrm{E}_1}^{\mathrm{CI}}$, $PL_{\mathrm{E}_2}^{\mathrm{CI}}$ and $PL_{\mathrm{P}_2}^{\mathrm{CI}}$ refer to the CI PL model modified with 1) the exponential function with a single term; 2) the exponential function with 2 terms and 3) the 2nd-order polynomial function, respectively. The A, B, C, and D terms are constant values to be computed. Nevertheless, further comprehensive outdoor snowstorm experiment campaigns are required to precisely establish the factors accountable to each exponential mode.

D. RELEVANCE TO FUTURE DEPLOYMENTS, LIMITATIONS AND FUTURE WORK

The study's findings have crucial relevance for the deployment of mmWave communication networks in areas like northern parts of North America and Northern Central Asia, where snowstorms and other extreme weather circumstances are common. In such environments, the modified PL equations put forward in this study may be a useful tool for forecasting signal behavior and mitigating attenuation, improving network performance's robustness and reliability. Higher PL parameters of $PLE = 4.12$ and $\sigma^{\mathrm{CI}} = 9.32dB$ indicate a considerably steep rate of signal attenuation over distance and greater variability in the received signal power, which presents challenges to maintaining reliable connectivity in regions prone to snowstorms. Future link budget planning at 60 GHz mmWave systems shall consider these factors. To sustain adequate signal margins and smooth and wider coverage in the future 60 GHz mmWave systems, the network planners would need to use higher transmission powers and deployment of base stations at closer intervals. Though these observations are particularly important to the 60 GHz frequency, with further examination, they could potentially find wider use in other mmWave bands.

This study has certain limitations. The outdoor experiments were run in snowstorm circumstances with certain wind speeds, snowfall rates, and temperatures. Variability in these parameters may result in different PL behavior. The results are also limited to the 60 GHz spectrum, which is not directly applicable to other mmWave frequency bands like 28 or 73 GHz. The experimental design also overlooked urban environmental factors like buildings and cars, which might affect signal propagation in real-world deployments.

In future work, extending the investigations to other bands of 28 GHz and 73 GHz would provide a more comprehensive understanding of frequency-dependent propagation behaviors under snowstorms. Likewise, the applicability of PL research from snowstorms to dense urban deployments in the real world can be improved by analyzing small-scale fading effects induced by reflections and scattering of buildings, vehicles, and other urban variables. Moreover, to thoroughly examine the influence of each atmospheric factor separately, such as wind speed, snowfall rate, temperature, snowflake size, and humidity, snowstorm experiment campaigns must be continued under different circumstances. Furthermore, to obtain more accurate inferences on mmWave PL under snowstorms, antennas can be located beneath high canopies to protect them from precipitation. This way, the influence of both the snow moisture on antenna transmission and the canopies' influence on radiation patterns could be minimized.

Additionally, while snowstorm measurements were ensured to be conducted beyond the Fresnel region, future investigation could explore near-field effects, particularly for extremely large-scale antenna arrays (ELAA). Understanding near-field electromagnetic radiation behavior is crucial as ELAA becomes a vital aspect of mmWave and THz communication systems for 6G networks. ELAA's wide apertures and high frequencies require near-field spherical wave analysis instead of far-field assumptions. Understanding how snowfall conditions, including snowflake scattering, wind-driven dynamics, and environmental moisture, affect near-field radiation patterns can contribute to building resilient communication systems in harsh climates. Integrating these concerns with this study's PL modifications could boost mmWave system reliability and scalability under different deployment conditions.

V. CONCLUSION

This study highlighted the significant impact of snowfall, moisture content, and high wind speed on PL in wireless communication systems used outdoors in the 60 GHz band. It also provides practical contributions by proposing modified equations of the CI PL model in 60 GHz tailored for snowstorm conditions for improved signal prediction. These findings can be essential in designing robust 60 GHz mmWave communication systems in outdoor snow-prone territories. Furthermore, this research adds to the theoretical knowledge of mmWave signal propagation by verifying the adverse impact of snowfall rate, wind speed, and humidity on PL. Particularly these impacts reveal a 15 dB higher snowstorm PL at a 1-meter T-R distance compared to indoors. This difference decreases by half at a 7-meter T-R distance. Beyond the 7-meter distance, the experimental snowstorm PL exhibited exponential growth. It was also revealed that the 60 GHz snowstorm PL can be reasonably approximated by the two-term exponential function. The comparably high accuracy of the two-term exponential modification also suggested the existence of two distinct exponential growth modes in the PL data. Though the second-order polynomial modification showed the highest R^2 score, its application may be fraught with the risk of over-fitting.

REFERENCES

[1] T. S. Rappaport, S. Sun, R. Mayzus, H. Zhao, Y. Azar, and K. Wang, "Millimeter wave mobile communications for 5G cellular: It will work!" *IEEE Access*, vol. 1, pp. 335–349, 2013.

[2] *IEEE Standard for Information Technology–Telecommunications and Information Exchange Between Systems—Local and Metropolitan Area Networks–specific Requirements—Part 11: Wireless LAN Medium Access Control (MAC) and Physical Layer (Phy) Specifications*, IEEE Standard 802.11-2020 (Revision of IEEE Std 802.11-2016), 2021.

[3] R. W. Heath, "Millimeter wave: The future of commercial wireless systems," in *Proc. IEEE Compound Semicond. Integr. Circuit Symp. (CSICS)*, 2016, pp. 1–4.

[4] W. Hong, Z. H. Jiang, C. Yu, D. Hou, H. Wang, and C. Guo, "The role of millimeter-wave technologies in 5G/6G wireless communications," *IEEE J. Microw.*, vol. 1, no. 1, pp. 101–122, Jan. 2021.

[5] M. Xiao, S. Mumtaz, Y. Huang, L. Dai, Y. Li, and M. Matthaiou, "Millimeter wave communications for future mobile networks," *IEEE J. Sel. Areas Commun.*, vol. 35, no. 9, pp. 1909–1935, Sep. 2017.

[6] A. E. C. Redondi, C. Innamorati, S. Gallucci, S. Fiocchi, and F. Matera, "A survey on future millimeter-wave communication applications," *IEEE Access*, vol. 12, pp. 133165–133182, 2024.

[7] T. Bai and R. W. Heath, "Coverage and rate analysis for Millimeter-wave cellular networks," *IEEE Trans. Wireless Commun.*, vol. 14, no. 2, pp. 1100–1114, Feb. 2015.

[8] G. R. MacCartney and T. S. Rappaport, "73 GHz millimeter wave propagation measurements for outdoor urban mobile and backhaul communications in New York City," in *Proc. IEEE Int. Conf. Commun. (ICC)*, 2014, pp. 4862–4867.

[9] S. Dimce, M. S. Amjad, and F. Dressler, "mmWave on the road: Investigating the weather impact on 60 GHz V2X communication channels," in *Proc. 16th Annu. Conf. Wireless On-Demand Netw. Syst. Services Conf. (WONS)*, 2021, pp. 1–8.

[10] R. K. Garg and S. K. Soni, "Empirical path loss models at 433 MHz in Himalayan snow for health monitoring," *World J. Eng.*, vol. 19, no. 2, pp. 157–165, 2022.

[11] S. L. Javali, A. Torabi, and S. A. R. Zekavat, "Snow covered forest channel modeling for near-ground wireless sensor networks," in *Proc. IEEE Int. Conf. Wireless Space Extreme Environ. (WiSEE)*, 2017, pp. 69–74.

[12] K. Nakamura, N. Iwasawa, K. Kawasaki, S. Yoshida, and M. Takahashi, "The attenuation characteristics of millimeter-wave by snow accretion," *IEICE Commun. Exp.*, vol. 9, no. 12, pp. 674–678, 2020.

[13] M. Abdulali and S. Salous, "Snow attenuation measurement for short-range mmWave fixed link," in *Proc. 4th URSI Atlantic Radio Sci. Meeting (AT-RASC)*, 2024, pp. 1–4.

[14] C. Lai, D. Senic, C. Gentile, J. Senic, and N. Golmie, "Raytracing digital foliage at millimeter-wave: A case study on calibration against 60-GHz channel measurements on summer and winter trees," *IEEE Access*, vol. 11, pp. 145931–145943, 2023.

[15] R. Zavorka, T. Mikulasek, J. Vychodil, J. Blumenstein, A. Chandra, and H. Hammoud, "Characterizing the 80 GHz channel in static scenarios: Diffuse reflection, scattering, and transmission through trees under varying weather conditions," *IEEE Access*, vol. 12, pp. 144738–144749, 2024.

[16] X. Wu, C.-X. Wang, J. Sun, J. Huang, R. Feng, and Y. Yang, "60-GHz millimeter-wave channel measurements and modeling for indoor office environments," *IEEE Trans. Antennas Propag.*, vol. 65, no. 4, pp. 1912–1924, 2017.

[17] M. Kim, A. Ghosh, R. Takahashi, and K. Shibata, "Indoor channel measurement at 300 GHz and comparison of signal propagation with 60 GHz," *IEEE Access*, vol. 11, pp. 124040–124054, 2023.

[18] C. Amaya, J.-M. Garcàa-Rubia, P. Bouchard, and T. Nguyen, "Experimental assessment of snow-induced attenuation on an earth-space link operating at Ka-band," *Radio Sci.*, vol. 49, no. 10, pp. 933–944, 2014.

[19] Y. Amarasinghe, W. Zhang, R. Zhang, D. M. Mittleman, and J. Ma, "Attenuation of terahertz waves by wet snow, dry snow and rain," in *Proc. IEEE Int. Conf. Plasma Sci. (ICOPS)*, 2020, pp. 216–216.

[20] Q. Jing, D. Liu, and J. Tong, "Study on the scattering effect of terahertz waves in near-surface atmosphere," *IEEE Access*, vol. 6, pp. 49007–49018, 2018.

[21] (Millimeter Wave Product Inc., St. Petersburg, FL, USA). *WR-15 Standard Gain Horn Antennas*. (2024). [Online]. Available: https://www.miwv.com/v-band-standard-gain-horn-antennas-wr-15-50-75-ghz-5/

[22] "Climate and weather averages in Astana, Kazakhstan," Accessed: Jan. 15, 2025. [Online]. Available: https://www.timeanddate.com/weather/kazakstan/astana/climate

[23] G. R. Maccartney, T. S. Rappaport, S. Sun, and S. Deng, "Indoor office wideband millimeter-wave propagation measurements and channel models at 28 and 73 GHz for ultra-dense 5G wireless networks," *IEEE Access*, vol. 3, pp. 2388–2424, 2015.

[24] J. Karjalainen, M. Nekovee, H. Benn, W. Kim, J. Park, and H. Sungsoo, "Challenges and opportunities of mm-Wave communication in 5G networks," in *Proc. 9th Int. Conf. Cogn. Radio Oriented Wireless Netw. Commun. (CROWNCOM)*, 2014, pp. 372–376.

SATZHAN S. ASKAROV received the B.Eng. and M.Sc. degrees in electrical and computer engineering from Nazarbayev University, Astana, where he is currently pursuing the Ph.D. degree in electrical engineering with his alma mater. He worked as a Circuit Engineer on the production of hardware with audio and video solutions for industrial purposes. He joined the Integrated Device Solutions and Nanophotonics Laboratory, Nazarbayev University in 2022.

REFIK C. KIZILIRMAK (Senior Member, IEEE) received the B.Sc. and M.Sc. degrees in electrical and electronics engineering from Bilkent University, Ankara, Türkiye, in 2004 and 2006, respectively, and the Ph.D. degree from Keio University, Yokohama, Japan, in 2010. He worked on several telecommunication and defense industry projects with the Communications and Spectrum Management Research Center, Türkiye. He is currently with the Department of Electrical and Electronics Engineering, Nazarbayev University, Astana, Kazakhstan. He contributed to the technical requirements document of 802.15.7r1 standardization, which will enable visible light communication. He holds three patent applications in the field of wireless communications to U.S. and Japan patent offices. He was a recipient of the IEEE VTS Japan 2008 Young Researcher's Award and the IEICE WBS Best Paper Award.

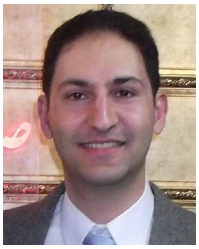

BEHROUZ MAHAM (Senior Member, IEEE) received the B.Sc. and M.Sc. degrees in electrical engineering from the University of Tehran, Iran, in 2005 and 2007, respectively, and the Ph.D. degree from the University of Oslo, Norway, in 2010.

From September 2008 to August 2009, he was with the Department of Electrical Engineering, Stanford University, Stanford, CA, USA. He is currently an Associate Professor with the ECE Department, School of Engineering, Nazarbayev University. He was an Assistant Professor with the School of Electrical and Computer Engineering, University of Tehran from September 2011 to September 2015. He has around 170 publications in major technical journals and conferences. His fields of interest include wireless communication and networking, signal processing for communications, Internet of Things, Beyond 5G, UAV, and satellite communications.

Dr. Maham is a TWAS Affiliate. He has been an Editorial Member of IEEE TRANSACTIONS ON COMMUNICATIONS, *Physical Communication* (Elsevier), and *Transactions on Emerging Telecommunications Technologies* (Wiley & Sons).

IKECHI AUGUSTINE UKAEGBU (Senior Member, IEEE) received the B.Eng. degree in electrical engineering, electromechanics, and electrotechnology and the M.Eng. degree in electronics and microelectronics from the Moscow Power Engineering Institute (National Research University), Moscow, Russia, in 2004 and 2006, respectively, and the Ph.D. degree from the Korea Advanced Institute of Science and Technology (KAIST) in 2012.

He was a "Brain Korea-21" Postdoctoral Fellow with the Electrical Engineering Department, KAIST from 2012 to 2013. From 2018 to 2024, he was an Assistant Professor with the Electrical and Computer Engineering Department, School of Engineering and Digital Sciences, Nazarbayev University. Since 2024, he has been an Adjunct Professor with the School of Professional Studies, Saint Louis University, St. Louis, MO, USA. He is currently an Assistant Professor with the Division of Engineering Technology, University of West Alabama, Livingston, AL, USA. In 2018, he founded the Integrated Device Solutions and Nanophotonics Laboratory, Nazarbayev University, where he is currently the Director. He held research and development positions with the Electronics and Telecommunications Research Institute, South Korea, from 2008 to 2009 and with Lightron Fiber-Optics Inc., South Korea, in 2013. He also worked as a Senior Engineer with the Design Technology Team, System LSI Division, Samsung Electronics Company Ltd., South Korea, from 2013 to 2016. He co-founded a venture startup company (Axinaux), where he served as the CTO/Product Development Manager in 2016. He has authored and co-authored over 100 research papers, including 38 peer-reviewed journals, 55 papers in conference proceedings. His research interests include circuits and systems, integrated silicon photonics, microwave photonics, optoelectronics, energy harvesting systems, and RF systems.

Dr. Ukaegbu is a reviewer of several journals, and has served as a TPC member in several IEEE Conferences.